Interaction-induced topological states of photon pairs

Andrei A. Stepanenko ◉ and Maxim A. Gorlach ◉*

Department of Physics and Engineering, ITMO University, Saint Petersburg 197101, Russia

To date, the concept of topological order relies heavily on the properties of single-particle bands. Only recently it has been realized that interactions can have a dramatic impact on topological properties, not only modifying the topology of the bands but also creating a topological order in an otherwise trivial system. Applying an extended version of the Bose-Hubbard model, we investigate a system which, being topologically trivial in the single-particle regime, harbors topologically nontrivial edge and interface states of repulsively bound photon pairs. Whereas binding of the photons in this model is captured by the standard local interaction term, an additional direct two-photon hopping renders the system topologically nontrivial. Besides their interaction-induced origin, predicted two-photon edge states exhibit a range of other unexpected features, including the robustness to collapse of the corresponding bulk band and the ability to coexist with the continuum of two-photon scattering states forming a bound state in the continuum. Performing rigorous calculation of the Zak phase for bound photon pairs, we prove the topological origin of the two-photon edge states.

I. INTRODUCTION

Topological photonics offers a rich variety of remarkable functionalities including disorder-robust routing of light on a chip [1–6]. While topological states in classical optical systems form an established area of research [1–6], the emphasis is currently shifting towards topological states of quantum light [7–12] with the potential of applications in topologically protected quantum information transfer, quantum computations, and manipulation of entangled photons with quantum metasurfaces [13].

Within just one year, the first realizations of single-photon topological states [8,9] and topologically protected sources of nonclassical light [10] have been reported. Moreover, previous theoretical analysis of entangled photon propagation in a topological system [14,15] has been followed by recent experiments [11,12]. In this context, it is especially important to investigate the implications of topological protection for more complex quantum states of light which can potentially uncover further exciting applications of topological photonics.

One such intriguing state of quantum light is represented by doublons, which are bound photon pairs arising in discrete nonlinear arrays due to repulsive Kerr-type nonlinearity [16,17]. Quite counterintuitive properties of doublon quasiparticles were analyzed in a series of theoretical papers in the context of bulk [18–22] and edge [23–29] doublon states including more advanced concepts of doublons in two-dimensional (2D) geometries [30,31], Thouless pumping of doublons [32,33], and dissipatively bound photon pairs [34].

Driven by the ambitious goal to realize topological doublon edge states, we and several other groups have investigated the well-celebrated Su-Schrieffer-Heeger (SSH) model [35] in the two-photon regime with an effective on-site repulsive photon-

photon interaction [36–38]. However, since the analyzed model is topologically nontrivial even in the single-particle case, the emergence of two-photon edge states [37] is not so surprising. Therefore, it is much more exciting to demonstrate topological states of doublons induced by interactions in an otherwise topologically trivial system.

Interestingly, such interaction-induced topological states are already known for classical systems characterized by intensity-dependent coupling constants between some of the sites which give rise to self-induced topological transitions [39–41]. To demonstrate interaction-induced topological states of photon pairs, we have recently proposed [42] a one-dimensional (1D) system which includes two main ingredients: on-site interactions to ensure the formation of bound photon pairs and direct two-photon hopping incorporated between the sites of the system in an alternating manner [Fig. 1(a)]. Note that the latter mechanism does not affect single-particle eigenstates and energies becoming effective in
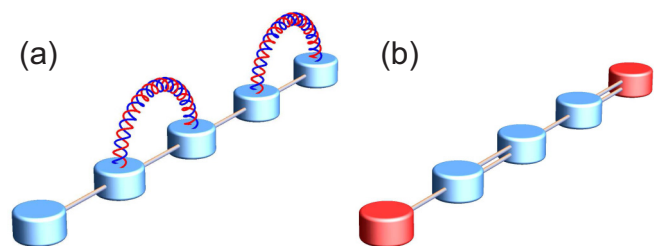

FIG. 1. (a) Sketch of the system under study. Straight connecting lines represent the single-photon tunneling amplitude J, whereas wavy lines illustrate direct two-photon hopping P, which enters the extended Bose-Hubbard Hamiltonian Eq. (1). (b) In the limit of strong interactions $U \gg J$ the dynamics of a bound photon pair is governed by the effective Su-Schrieffer-Heeger model, with the detuned edge resonators highlighted in red.

*m.gorlach@metalab.ifmo.ru

the presence of two photons, while the alternating pattern of the two-photon hoppings renders our system analogous to the well-celebrated SSH model with two sites in the unit cell [Fig. 1(b)].

In this article, we investigate and advance the concept of interaction-induced topological doublon states in the presence of direct two-photon hopping, deriving the dispersion of bulk doublons and calculating the Zak phase for them. Our results prove the topological origin of the interaction-induced doublon states and provide valuable insights into the problem of topological characterization of few-body states. Quite importantly, topological states of doublons studied here should not be mixed with solitonlike nonlinear topological states of classical light arising in waveguide lattices with Kerr-type nonlinearity [43,44] or mean-field solutions of the nonlinear Gross-Pitaevskii equation in the form of vortices [45] because of the few-body nature of topological states in our proposal.

The rest of the paper is organized as follows. In Sec. II we summarize our model and provide simple arguments to prove the existence of interaction-induced topological states. Section III contains an in-depth analysis of the bulk properties of bound photon pairs including an analytical model for their dispersion and diagrams showing the evolution of doublon bands when the parameters of the model are varied. The properties of the edge and interface doublon states are examined in Sec. IV, whereas our conclusions and outlook for future studies are reported in Sec. V. Technical details regarding calculation of the bulk doublon dispersion and Zak phase are summarized in Appendixes A and B, respectively, while Appendix C discusses the distinction between trivial and topological doublon edge states.

II. SUMMARY OF THE MODEL AND DOUBLON EDGE STATES

We search for the eigenstates of the system described by the extended version of the Bose-Hubbard Hamiltonian:

$$
\begin{aligned}
\hat{H} = {} & \omega_0 \sum_m \hat{n}_m - J \sum_m (\hat{a}_m^\dagger \hat{a}_{m+1} + \hat{a}_{m+1}^\dagger \hat{a}_m) \\
& + U \sum_m \hat{n}_m (\hat{n}_m - 1) \\
& + \frac{P}{2} \sum_m (\hat{a}_{2m}^\dagger \hat{a}_{2m}^\dagger \hat{a}_{2m+1} \hat{a}_{2m+1} + \text{H.c.}),
\end{aligned}
\tag{1}
$$

where we assume that $\hbar = 1$, $\hat{a}_m^\dagger$ and $\hat{a}_m$ are creation and annihilation operators for the photon in the mth cavity, $\hat{n}_m = \hat{a}_m^\dagger \hat{a}_m$ is a local photon number operator, ω_0 is a cavity eigenfrequency, and J is the photon tunneling amplitude. The term $\propto U$ describes local photon-photon interaction mediated by the nonlinearity of the medium, whereas the additional term $\propto P$ captures direct two-photon hopping. The latter two terms, obviously, do not come into play provided single-particle dynamics is studied, and hence no single-photon topological states are expected.

What is more remarkable, however, is the two-particle sector of this Hamiltonian. It is straightforward to verify that the Hamiltonian Eq. (1), conserves the number of particles and thus the two-photon wave function can be searched in the

form

$$
|\psi\rangle = \frac{1}{\sqrt{2}} \sum_{m,n} \beta_{mn} \hat{a}_m^\dagger \hat{a}_n^\dagger |0\rangle
\tag{2}
$$

with the usual normalization $\langle \psi | \psi \rangle = 1$ and unknown superposition coefficients β_{mn}. As a consequence of bosonic symmetry, $\beta_{mn} = \beta_{nm}$ for any indices m and n. Inserting Eqs. (1) and (2) into the Schrödinger equation

$$
\hat{H} |\psi\rangle = (\varepsilon + 2\,\omega_0) |\psi\rangle,
$$

with $2\,\omega_0$ used as an energy reference, we derive the linear system of equations:

$$
(\varepsilon - 2U)\beta_{2m,2m} = -2J\beta_{2m+1,2m} - 2J\beta_{2m,2m-1} + P\beta_{2m+1,2m+1},
\tag{3}
$$

$$
\begin{aligned}
(\varepsilon - 2U)\beta_{2m+1,2m+1} = {} & -2J\beta_{2m+2,2m+1} \\
& - 2J\beta_{2m+1,2m} + P\beta_{2m,2m},
\end{aligned}
\tag{4}
$$

$$
\varepsilon \beta_{m,n} = -J\beta_{m+1,n} - J\beta_{m-1,n} - J\beta_{m,n+1} - J\beta_{m,n-1} \quad (m \neq n).
\tag{5}
$$

In the case of a finite array of length N we additionally impose open boundary conditions $\beta_{00} = \beta_{m0} = 0$ and $\beta_{N+1,N+1} = \beta_{m,N+1} = 0$ with $m = 1, 2, \dots N$. As pointed out in Refs. [27], [36], and [37], these equations can be reinterpreted as an eigenvalue problem for the single particle in a 2D tightbinding lattice. In the latter model, photon-photon interactions U are emulated by the detuning of the resonance frequency for the diagonal cavities, whereas the two-photon hopping P is represented as an additional coupling between the diagonal sites.

While the outlined 1D two-particle model can be implemented with optical lattices [46] or with arrays of transmon qubits [47–49], the range of parameters attainable in both types of realization is quite limited, the constraints on the magnitude of direct two-photon hopping being especially strict [46,50]. However, in view of the discussed 1D-2D mapping, the same physics can be emulated with 2D classical arrays free of such limitations [51], including, for instance, coupled waveguide lattices [52] or LC circuits [42]. Therefore we do not restrict our analysis by a particular realization of the proposed model and examine the arbitrary ratios U/J and P/J revealing a full plethora of available effects. The only assumption that is made is the repulsive nature of nonlinearity, $U > 0$. The spectrum for $U < 0$ is immediately recovered by calculating the two-photon states for the system with parameters $-U$ and $-P$ and by inverting the sign of the derived energy. Furthermore, to analyze both possible terminations of the array simultaneously, we focus our attention on the case of odd N when the array starts and terminates with different tunneling links.

To grasp the main features of the proposed system, we start from a simplified model valid in the limit $U \gg J$. In this *strong-interaction limit* the doublons are tightly bound, i.e., β_{mm} coefficients are the dominant ones in the expansion Eq. (2). As such, we can rewrite the system Eqs. (3)–(5) in terms of β_{mm} coefficients, treating $\beta_{m+1,m}$ as a perturbation and fully neglecting the coefficients $\beta_{m+p,m}$ for $p \geqslant 2$. This

approach yields the eigenvalue problem,

$$(\varepsilon - 2U - 2j)\beta_{2m,2m} = j\beta_{2m-1,2m-1} + (j+P)\beta_{2m+1,2m+1},$$
(6)

$$(\varepsilon - 2U - 2j)\beta_{2m+1,2m+1} = (j+P)\beta_{2m,2m} + j\beta_{2m+2,2m+2},$$
(7)

with the boundary conditions

$$(\varepsilon - 2U - j)\beta_{11} = j\beta_{22},$$
(8)

$$(\varepsilon - 2U - j)\beta_{N,N} = (j+P)\beta_{N-1,N-1},$$
(9)

where $j = J^2/U$ is the effective doublon hopping rate associated with two consecutive single-particle tunnelings to the neighboring cavity.

Equations (6) and (7) suggest that in the strong-interaction limit the dynamics of a doublon is governed by the SSH Hamiltonian [35] as illustrated in Fig. 1(b). This model is known to give rise to the two topologically nontrivial bands with the dispersion

$$\varepsilon_{\pm}(k) = 2U + 2j \pm \sqrt{j^2 + (j+P)^2 + 2j(j+P)\cos 2k}.$$
(10)

Here, periodic boundary conditions are implied and the Bloch wave number k is defined such that the first Brillouin zone spans the range $[-\pi/2, \pi/2]$. According to Eq. (10), the bandgap closing occurs for $|j+P| = |j|$, since this condition renders the two tunneling amplitudes equal. Specifically, for $P = 0$ and

$$P = -2J^2/U$$
(11)

the bandgap closes at $k = \pm\pi/2$ and $k = 0$, respectively.

Furthermore, under a suitable parameter choice, doublon bands can be made dispersionless. As a condition for the flat band, we require that $\varepsilon_{+}(0) = \varepsilon_{+}(\pi/2)$, i.e., $|2j + P| = |P|$, which can happen in two situations: (i) the trivial case $P \gg j$ or $UP \gg J^2$, which implies both strong photon-photon interaction and strong two-photon hopping, and (ii) the nontrivial case where $j + P = 0$ or

$$P = -J^2/U.$$
(12)

In the latter case half of the tunneling links in the array vanish, turning it into a collection of uncoupled dimers.

Besides the intuition about the properties of bulk doublon bands, the developed model also provides some insights into the properties of edge and interface states. While in the canonical SSH model the edge state arises at the center-of-bandgap frequency being localized at the weak-link edge, this case is a bit different because of the interaction-induced detuning of the edge sites by j evident from the comparison of Eqs. (6) and (7) vs (8) and (9).

Solving Eq. (9) together with Eqs. (6) and (7) for $N \gg 1$, we do not find any localized states near site (N, N). At the same time, a similar analysis for the $(1,1)$ site yields two states with the degree of localization given by

$$z_{1,2} = e^{2ik} = \frac{j+P}{2j^3}[2jP + P^2 \pm \sqrt{(2jP + P^2)^2 + 4j^4}],$$
(13)

where localized states correspond to $|z| < 1$. The energies of the edge states read

$$\varepsilon_{1,2} = 2U + j - \frac{1}{2j}[2jP + P^2 \pm \sqrt{(2jP + P^2)^2 + 4j^4}].$$
(14)

Equation (13) shows that the higher-energy state ε_2 is localized for any $P \neq 0$, while the lower-energy state ε_1 is possible provided that

$$-\frac{2J^2}{U} < P < 0.$$
(15)

Equation (15) is equivalent to the condition $j > |j + P|$, which guarantees that the $(1,1)$ site is the strong-link edge. Hence, for parameter values given by Eq. (15), both of the edge states are trivial. In the opposite case, $P > 0$ or $P < -2J^2/U$, site $(1,1)$ becomes a weak-link edge and supports a single state with energy ε_2. Thus, for P outside of the interval Eq. (15) state ε_2 is a topological one, transforming to a trivial state when the condition Eq. (15) is fulfilled. State ε_1 is always a trivial state. Note also that the boundaries of the interval in Eq. (15) coincide with the points of closing and reopening of a bandgap between two doublon bands, which illustrates the bulk-boundary correspondence for the two-photon topological states in the strong-interaction limit.

To further exemplify the topological nature of the two-photon modes, we analyze interface states localized at the defect formed by the two repeated tunneling links, which can be viewed as the boundary of two 1D arrays with opposite dimerizations. If, for instance, the interface defect is formed by the two repeated tunneling links j, similarly to the reasoning above we obtain the interface condition in the form

$$(\varepsilon - 2U - 2j)\beta_{00} = j(\beta_{11} + \beta_{-1,-1}),$$
(16)

while two repeated $j + P$ links (Fig. 3) yield the interface condition:

$$(\varepsilon - 2U - 2j)\beta_{00} = (j+P)(\beta_{11} + \beta_{-1,-1}).$$
(17)

Hence, the interface site is not detuned with respect to the bulk ones [cf. Eqs. (6) and (7)], and as a consequence the topological interface state is located exactly in the middle of the bandgap $\varepsilon_{\text{int}} = 2U + 2j$. If the interface defect is formed by the two consecutive strong links, the topological state is also accompanied by two trivial modes lying outside of the doublon bandgap [53].

The developed model is only valid in the limit of $U \gg J$. In Sec. III we derive a rigorous solution for the dispersion of bound photon pairs based on the Bethe ansatz method and capture a range of intriguing phenomena beyond the canonical SSH model including the interaction of doublon bands with the continuum of scattering states.

III. DISPERSION OF BULK DOUBLONS

To solve an infinite set of equations (3)–(5), and extract the dispersion of photon pairs, one needs some analytic expression for β_{mn} coefficients. A powerful approach to this problem is provided by the Bethe ansatz technique [54,55].

The standard Bethe ansatz has the form

$$\beta_{mn} = C \exp\left[i\frac{k}{2}(m+n) + i\frac{\varkappa}{2}(m-n)\right] \qquad (18)$$

for $m \geqslant n$. In this expression, k is the Bloch wave number describing the motion of the photon pair as a whole, whereas $\varkappa$ captures the relative motion of particles. Bound photon pairs are characterized by a complex $\varkappa$, in which case the wave function decays with the increase in separation $(m - n)$ between the photons.

While this simple ansatz captures the properties of bound pairs in the limiting case $P = 0$, it is inconsistent with Eqs. (3)–(5) in the general case of $P \neq 0$ and arbitrary k. To proceed with the analytical solution, we need to incorporate into the ansatz the presence of *two* sites in the unit cell. This extended unit cell shrinks the first Brillouin zone for doublons from $[-\pi, \pi]$ (as is the case for $P = 0$) to $[-\pi/2, \pi/2]$, mixing the states with wave numbers k and $k + \pi$. Therefore, we introduce the following modification of the Bethe ansatz:

$$\beta_{mn} = C_1\, e^{ik(m+n)/2}\, e^{i\varkappa_1(m-n)/2}$$
$$+ C_2\, e^{i(k+\pi)(m+n)/2}\, e^{i\varkappa_2(m-n)/2} \qquad (19)$$

with $m \geqslant n$ and $\operatorname{Im} \varkappa_{1,2} > 0$. The modified ansatz Eq. (19) appears to be consistent with the full system of equations (3)–(5), and determines the doublon dispersion as further detailed in Appendix A.

Omitting the details of the derivation, we would like to stress here several simple but illuminating results. The energies of doublon bands in the limiting case $k = \pm\pi/2$ can be found analytically:

$$\varepsilon_+ = \operatorname{sgn}[2U + P]\sqrt{(2U + P)^2 + 8J^2}, \qquad (20)$$

$$\varepsilon_- = \operatorname{sgn}[2U - P]\sqrt{(2U - P)^2 + 8J^2}. \qquad (21)$$

Thus, bound photon pairs are always stable for wave numbers near the boundaries of the first Brillouin zone. In the strong-interaction limit, the energies of the two bands scale as $(2U + P)$ and $(2U - P)$, which means that the effective photon-photon interaction U defines the average energy of the bound pair, whereas the two-photon hopping P controls energy splitting between the two bands.

For $k = 0$, the energies of the doublon states read

$$\varepsilon'_+ = \operatorname{sgn}[2U + P]\sqrt{(2U + P)^2 + 16J^2}, \qquad (22)$$

$$\varepsilon'_- = 2U - P, \qquad (23)$$

where ε_- and ε'_- (ε_+ and ε'_+) can correspond to the same or to different doublon bands. Note that Eqs. (20)–(23) agree with the simplified model Eq. (10), up to first order in j. Furthermore, the doublon band associated with ε'_- can collapse, intersecting with the continuum of two-photon scattering states for nonzero k sufficiently far from the Brillouin zone boundaries. As we show in Appendix A, collapse of the doublon band occurs in the range of parameters

$$-4J < 2U - P < 4J. \qquad (24)$$

To illustrate the obtained solution further, we explore the dispersion of doublons in two characteristic situations with the same two-photon hopping $P/J = -0.5$ and different

magnitudes of the effective photon-photon interaction: strong interactions $U/J = 6$ [Fig. 2(a)], and moderate interactions $U/J = 1$ [Fig. 2(b)]. The former case, shown in Fig. 2(a), exhibits a remarkable agreement with the effective SSH model [Eq. (10)], in terms of both the boundaries of the upper $12.5 < \varepsilon_{\mathrm{up}}/J < 12.8$, and lower $11.8 < \varepsilon_{\mathrm{l}}/J < 12.2$, bulk bands and the spectral position of the topological edge state $\varepsilon_{\mathrm{edge}}/J \simeq 12.2$. However, when the strength of the interaction U is decreased, one of the doublon bands intersects with the continuum of scattering states and collapses [Fig. 2(b)]. In agreement with our previous analysis, both doublon bands are stable near the edges of the Brillouin zone, while one of the bands becomes unstable in the vicinity of $k = 0$. At the same time, the edge states near the first site persist, coexisting with the continuum of scattering states.

It is also instructive to trace the evolution of doublon bands when the parameters of the model U and P are varied. The situation with a fixed P is illustrated in Fig. 2(c). In accordance with Eqs. (20) and (21), we observe that the continuum of scattering states can be located right between two doublon bands provided $(2U + P)$ and $(2U - P)$ have different signs, which happens for $U/J < 0.2$. The decreased spectral width of the lower band inside the continuum of scattering states for $0.3 < U/J < 1.75$ serves as evidence of doublon collapse. In agreement with the simplified model developed in Sec. II, doublon bands become dispersionless for $U/J = 2$ [cf. Eq. (12)] and the gap between them closes at $U/J = 4$ [cf. Eq. (11)]. In fact, such close agreement is not occasional, since the conditions for the flat band and for gap closing predicted by the simplified model coincide with those obtained from the rigorous solution as discussed in Appendix A.

In the strong-interaction limit, two-photon hopping P is the only parameter controlling the separation of two doublon bands. Figure 2(d) shows an almost linear dependence of doublon energies on the magnitude of P featuring two band touching points. This indicates closing and reopening of the bandgap as discussed in Sec. II and hints towards the topological transitions occurring in the system. For other parameters, we observe that the width of doublon bands decreases to 0, giving rise to the flat bands anticipated from our analysis in Sec. II. The situation appears to be more complicated for moderate interactions $U/J = 1$, when doublon bands interact with the scattering continuum collapsing and reviving [Fig. 2(e)]. In this case, the scattering continuum occupies the doublon bandgap for most of the considered values of P.

The doublon state with energy $(2U - P)$, shown by the dashed red line in Figs. 2(c) and 2(e), appears to be especially robust crossing the entire scattering continuum. The stability of this state is explained by the structure of its wave function $|\psi\rangle = (2N)^{-1/2}\sum_n (-1)^n \hat{a}_n^\dagger \hat{a}_n^\dagger |0\rangle$, which includes only states with two photons sharing the same cavity and which does not overlap with the remaining Fock states $\hat{a}_m^\dagger \hat{a}_n^\dagger |0\rangle$ ($m \neq n$). As a result, this doublon mode is a typical symmetry-protected bound state in the continuum (BIC) [56].

IV. EDGE AND INTERFACE TOPOLOGICAL DOUBLON STATES

The closing and reopening of a bandgap between two doublon bands demonstrated in Sec. III hints at topological
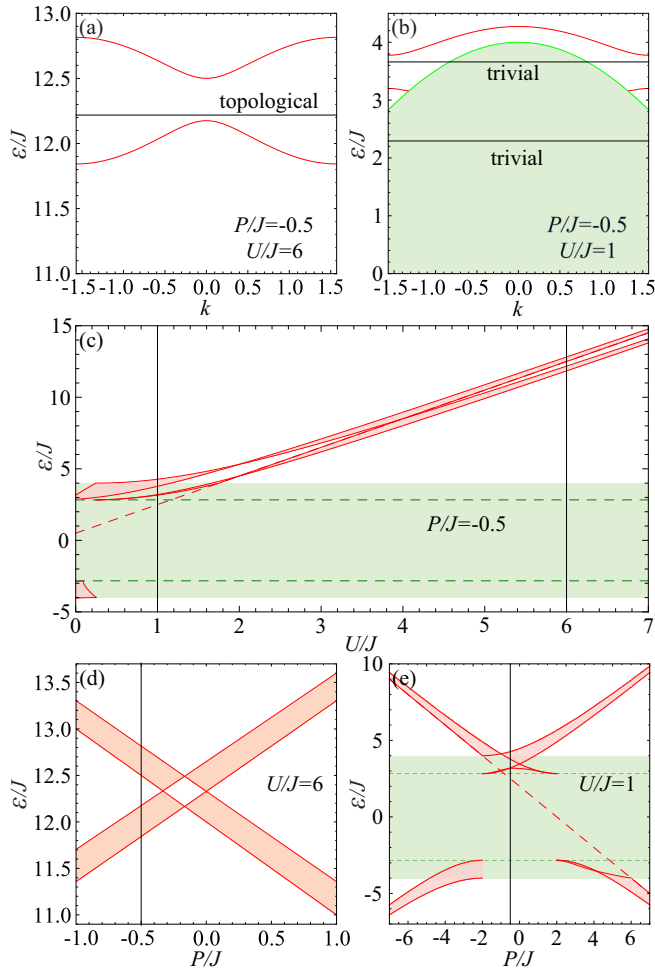
FIG. 2. Dispersion of two-photon excitations in the extended Bose-Hubbard model Eq. (1). Doublon dispersion for two representative cases: (a) the strong-interaction limit $U/J = 6$, $P/J = −0.5$; and (b) moderate interactions $U/J = 1$, $P/J = −0.5$. While the lower doublon band collapses, intersecting with the continuum of scattering states, two trivial doublon edge states, shown by black horizontal lines, coexist with the scattering continuum shown in light green. (c) Evolution of doublon bands shown in red when two-photon hopping $P/J = −0.5$ is fixed and the interaction strength U is varied. Vertical black lines indicate the values of U used in (a) and (b). The green band shows the range of energies of the two-photon scattering states when they exist for all k (between dashed green lines) or only for some k (above and below dashed green lines). [(d),(e)] Evolution of doublon bands when the photon-photon interaction U/J is fixed and the two-photon hopping P/J is varied. Vertical lines indicate the magnitude of P corresponding to (a) and (b). (d) Strong interactions $U/J = 6$. (e) Moderate interactions $U/J = 1$. The dashed red line in (c) and (e) shows the energy $2U − P$ of the doublon state coexisting with the continuum.

transitions occurring in the system. While the strong-interaction limit $U \gg J$ is well understandable in terms of the effective SSH-type model, the case of moderate interaction appears to be less intuitive. A characteristic example is presented in Fig. 2(b), where one of the doublon bands partially collapses and the edge state appears in the continuum of scattering states. These observations demonstrate two important features of our system.

First, the problem of bulk-boundary correspondence in two-particle topological models becomes more involved, since the corresponding doublon band can collapse, leaving the Berry connection undefined, whereas the topological state persists. Second, similarly to the bulk state $\varepsilon = 2U − P$ discussed above, the two-particle bound edge state can coexist with the continuum of scattering states as has been previously pointed out for a different two-particle model [25,26] providing a realization of the two-particle BIC [56].

To gain further intuition about the doublon BIC arising in this system, we analyze two geometries: (i) a finite array with the edge state localized near the first site and (ii) a domain wall between the two arrays with different dimerizations hosting the interface state. In the first scenario, illustrated in Figs. 3(a)–3(d), we observe two edge states of bound photon pairs. The state with a higher energy, shown in Figs. 3(a) and 3(b), still retains quite good localization close to exponential. At the same time, the lower-energy state [Figs. 3(c) and 3(d)], which lies deeper in the scattering continuum, clearly exhibits nonexponential localization caused by the stronger interaction with the continuum. In turn, the interface state [Fig. 3(e)] exhibits a symmetric profile with respect to the domain wall, thus resembling the interface state at a defect formed by two consecutive tunneling links in the canonical SSH model [53]. However, in contrast to the SSH case, the localization of the interface state is nonexponential [Fig. 3(f)] due to its hybridization with the scattering states.

To examine the topological protection of the predicted doublon edge and interface states, we evaluate the topological invariant for bound photon pairs. While the definition of topological invariants in multiparticle systems is generally a complicated task, the doublon can be viewed as an effectively one-dimensional quasiparticle and hence the standard Zak phase [57] can be calculated. However, the problem here is that the unit cell for the doublon includes an infinite set of the two-photon Fock states illustrated in Fig. 4(a). Whereas the center-of-mass position $(m + n)/2$ for these states is restricted by the interval $[−1/2; 3/2]$ [Fig. 4(a)], the separation between the two photons can take any values from 0 to ∞. Still, the unit cell can be chosen to be inversion symmetric, which ensures that the Zak phase γ can take only two values modulo 2π: either 0 or π [57].

We evaluate the Zak phase for the full range of U and P parameters encoding the value of the topological invariant by color in Fig. 4(c): the red-shaded area corresponds to $\gamma = \pi$ and the rest of the domain corresponds to $\gamma = 0$. This means that in the absence of interaction-induced detuning of the edge sites, the (N, N) site of the array hosts the edge state for U and P, which fall in the domain with $\gamma = \pi$.

As is typical for 1D systems, the Zak phase depends on the unit cell choice. For instance, if we shift the unit cell by a half-period such that its boundaries are given by the lines $m + n = 1$ and $m + n = 5$, the Zak phase will take the opposite value: $\gamma' = \gamma − \pi \mod 2\pi$ (see details in Appendix B). Hence, in the absence of interaction-induced detuning, the edge site $(1,1)$ of the array hosts the topological edge state for those U and P values which fall in the range $\gamma' = \pi$ ($\gamma = 0$), i.e., do not satisfy the inequality Eq. (15).

Thus, for any parameters U and P, one could expect a single topological edge state on one or another edge
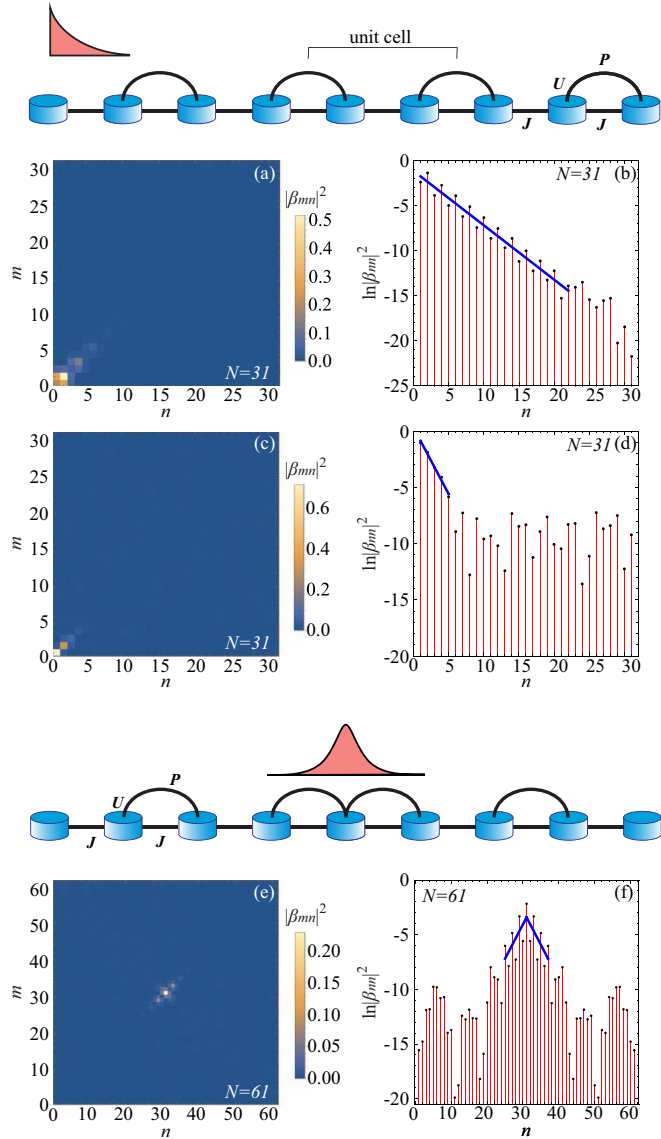
FIG. 3. Realization of doublon edge and interface states in the continuum for two geometries illustrated in insets. [(a),(c)] Probability distributions $|\beta_{mn}|^2$ for trivial doublon edge states localized near the first site of the array of the $N = 31$ cavity with energies $\varepsilon^{(\text{edge})}/J = 3.66$ and $\varepsilon^{(\text{edge})}/J = 2.29$, respectively. [(b),(d)] Probability distributions $|\beta_{nn}|^2$ versus n at logarithmic scale for the same states as in (a) and (c), respectively. Both edge states feature nonexponential localization. (e) Probability distribution for topological interface state of a doublon with energy $\varepsilon^{(\text{int})}/J = 3.53$ localized at the boundary between the two arrays with different dimerizations and overall length of the $N = 61$ cavity. (f) Probability distribution $|\beta_{nn}|^2$ versus n at logarithmic scale for the interface state in (e). The decay of the interface state with distance is not captured by a simple exponential formula. The calculations are performed for $U/J = 1$, $P/J = -0.5$ as in Fig. 2(b).

of the array. However, both edges of the array do experience an interaction-induced detuning equal to $j = J^2/U$ in the strong-interaction limit. As we discuss in detail in Appendix C, this detuning destroys the topological edge state at the Nth site and gives rise to the trivial states localized near the first site of the array.
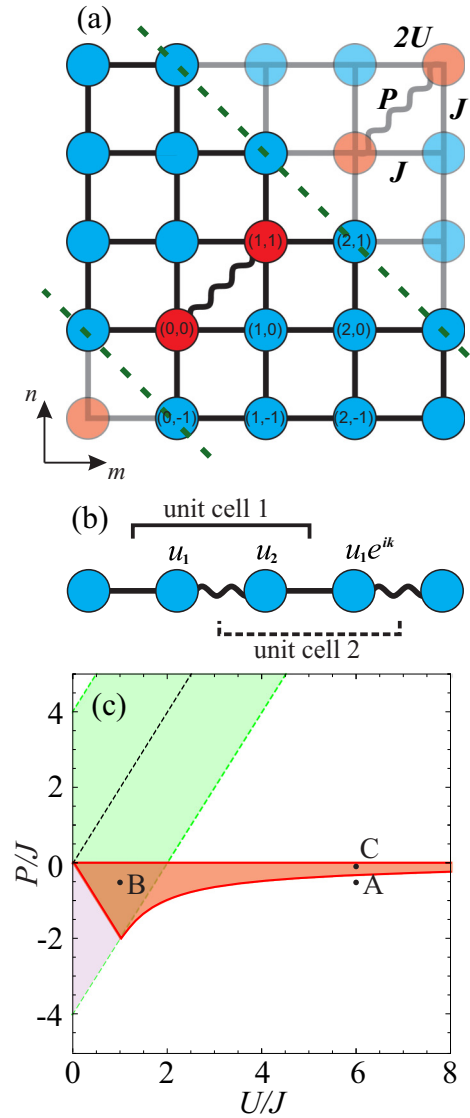

FIG. 4. (a) Illustration of various two-photon Fock states $\hat{a}_m^\dagger \hat{a}_n^\dagger |0\rangle$ comprising the two-photon wave function on a 2D map. Boundaries of the inversion-symmetric unit cell used for the Zak phase calculation for doublon bands are shown by dashed green lines. (b) Sketch of the reduced 1D model. Two choices of the unit cell are demonstrated. $u_{1,2}$ are the components of the wave function. (c) Phase diagram showing the magnitude of the Zak phase as a function of the model parameters U/J and P/J calculated for the unit cell choice shown in (a). The Zak phase is equal to π in the red-shaded area of the diagram and equal to 0 elsewhere. Areas shaded in light green and light purple indicate the parameters giving rise to the collapse of lower and upper doublon bands, respectively. The dashed black line corresponds to the condition $P = 2U$. Points A, B, and C mark the parameters corresponding to Fig. 2(a), Fig. 2(b), and Fig. 5(b), respectively.

V. DISCUSSION AND CONCLUSIONS

To summarize, we have investigated a system with interaction-induced topological order. Even though the single-particle model is topologically trivial, the two-particle bands feature a topological bandgap with doublon edge and interface states inside it. Quite interestingly, the observed two-particle

edge states remain stable under the collapse of the bulk doublon band, and moreover, they can coexist with the scattering continuum, providing a realization of the two-photon interaction-induced BIC.

By performing rigorous calculation of the Zak phase, we have revealed the topological transitions occurring in this system and have extended the bulk-boundary correspondence principle towards our interacting two-particle model.

We believe that the physical realization of the proposed model can be based on cold atomic gases in optical lattices, arrays of coupled transmon qubits, or other systems featuring a significant anharmonicity of the on-site potential. At the same time, mapping of the interacting 1D two-body problem onto the 2D classical setup possible for the class of Bose-Hubbard models opens another experimentally feasible route to probe the topological states in interacting systems.

APPENDIX A: CALCULATION OF THE BULK DOUBLON DISPERSION

In this Appendix, we outline the rigorous solution for the dispersion of bulk doublons based on the modified Bethe ansatz Eq. (19). We seek the solution of the equations

$$\varepsilon \beta_{m,n} = -J\beta_{m+1,n} - J\beta_{m-1,n}$$
$$- J\beta_{m,n+1} - J\beta_{m,n-1} \ (m \neq n), \quad \text{(A1)}$$

$$(\varepsilon - 2U)\beta_{2m,2m} = -2J\beta_{2m+1,2m}$$
$$- 2J\beta_{2m,2m-1} + P\beta_{2m+1,2m+1}, \quad \text{(A2)}$$

$$(\varepsilon - 2U)\beta_{2m+1,2m+1} = -2J\beta_{2m+2,2m+1}$$
$$- 2J\beta_{2m+1,2m} + P\beta_{2m,2m}, \quad \text{(A3)}$$

assuming that

$$\beta_{mn} = C_1\, e^{ik(m+n)/2}\, e^{i\varkappa_1(m-n)/2}$$
$$+ C_2\, e^{i(k+\pi)(m+n)/2}\, e^{i\varkappa_2(m-n)/2} \quad \text{(A4)}$$

for any $m \geqslant n$ and $\mathrm{Im}\,\varkappa_{1,2} > 0$. Inserting Eq. (A4) into the system Eqs. (A1)–(A3), we get

$$\varepsilon = -4J\,\cos\frac{k}{2}\,\cos\frac{\varkappa_1}{2}, \quad \text{(A5)}$$

$$\varepsilon = 4J\,\sin\frac{k}{2}\,\cos\frac{\varkappa_2}{2}, \quad \text{(A6)}$$

$$C_1\left[\varepsilon - 2U + 4J\,\cos\frac{k}{2}\,e^{i\varkappa_1/2} - P\,e^{ik}\right]$$
$$+ C_2\left[\varepsilon - 2U - 4J\,\sin\frac{k}{2}\,e^{i\varkappa_2/2} + P\,e^{ik}\right] = 0, \quad \text{(A7)}$$

$$C_1\left[\varepsilon - 2U + 4J\,\cos\frac{k}{2}\,e^{i\varkappa_1/2} - P\,e^{-ik}\right]$$
$$+ C_2\left[\varepsilon - 2U - 4J\,\sin\frac{k}{2}\,e^{i\varkappa_2/2} + P\,e^{-ik}\right] = 0. \quad \text{(A8)}$$

Here, Eqs. (A5) and (A6) are obtained from the single Eq. (A1) due to the linear independence of $e^{i\varkappa_1(m-n)/2}$ and $e^{i\varkappa_2(m-n)/2}$ for $m \neq n$. The system of four equations (A5)–(A8), defines four unknowns — ε, $\varkappa_1$, $\varkappa_2$, and the ratio C_1/C_2 — while the absolute values of C_1 and C_2 are determined from the normalization of the two-photon wave function.

Excluding the doublon energy from Eqs. (A7) and (A8) with Eqs. (A5) and (A6) and further rearranging them, we arrive at the linear system with respect to C_1 and C_2:

$$C_1\left[4iJ\,\cos\frac{k}{2}\,\sin\frac{\varkappa_1}{2} - 2U - P\,\cos k\right] + iC_2 P\,\sin k = 0, \quad \text{(A9)}$$

$$- iC_1 P\,\sin k$$
$$+ C_2\left[-4iJ\,\sin\frac{k}{2}\,\sin\frac{\varkappa_2}{2} - 2U + P\,\cos k\right] = 0. \quad \text{(A10)}$$

Setting the determinant of this system to 0, we recover that

$$8J^2\,\sin k\,\sin\frac{\varkappa_1}{2}\,\sin\frac{\varkappa_2}{2} - 4iJ\,\cos\frac{k}{2}\,\sin\frac{\varkappa_1}{2}\,(2U - P\,\cos k)$$
$$+ 4iJ\,\sin\frac{k}{2}\,\sin\frac{\varkappa_2}{2}\,(2U + P\,\cos k) + 4U^2 - P^2 = 0. \quad \text{(A11)}$$

To provide an efficient numerical algorithm to calculate the dispersion of doublons, we introduce two auxiliary dimensionless variables:

$$x \equiv -i\cos\frac{k}{2}\,\sin\frac{\varkappa_1}{2}, \quad \text{(A12)}$$

$$y \equiv -i\sin\frac{k}{2}\,\sin\frac{\varkappa_2}{2}. \quad \text{(A13)}$$

Making use of Eqs. (A5), (A6), and (A11), we get the following closed-form system of equations:

$$f(x,y,k) \equiv x^2 - y^2 + \cos k = 0, \quad \text{(A14)}$$

$$g(x,y,k) \equiv -16J^2\,x\,y + 4Jx\,(2U - P\,\cos k)$$
$$- 4Jy\,(2U + P\,\cos k) + 4U^2 - P^2 = 0. \quad \text{(A15)}$$

Separating the real and imaginary parts for $\varkappa_1$ and $\varkappa_2$ and taking into account that $\mathrm{Im}\,\varkappa_{1,2} > 0$, we can show that the real parts of x, y, and ε satisfy the following condition:

$$\mathrm{sgn}\,\varepsilon = -\,\mathrm{sgn}\,x = \mathrm{sgn}\,y. \quad \text{(A16)}$$

Hence, to find the doublon dispersion one has to solve the system of algebraic equations (A14) and (A15) numerically, keeping only those pairs of x and y which satisfy an additional constraint Eq. (A16). The doublon energy is then given by

$$\varepsilon = -4J\,\mathrm{sgn}\,x\,\sqrt{\cos^2\frac{k}{2} + x^2}. \quad \text{(A17)}$$

Note that bound pairs coexist with the continuum of two-photon scattering states. The bulk dispersion of such states is

captured by the simple formula (A5), where both parameters k and $\varkappa$ are real.

In some limiting cases, the expression for the doublon energy simplifies considerably. For instance, if $k = \pm\pi/2$, $x = -(2U \pm P)/(4J)$, whereas the doublon energy

$$\varepsilon_\pm = \text{sgn}\,(2U \pm P)\sqrt{(2U \pm P)^2 + 8J^2}. \qquad (A18)$$

Hence, doublons with k at the edge of the Brillouin zone are always stable.

Another limiting case is $k = 0$ when one of the doublon bands has $C_2 = 0$ and the Bethe ansatz in the standard form Eq. (18), can be applied. In this case, the energy of this particular doublon band is given by

$$\varepsilon_+' = \text{sgn}(2U + P)\sqrt{(2U + P)^2 + 16J^2}, \qquad (A19)$$

whereas the second doublon solution corresponds to fully colocalized photons and has the energy

$$\varepsilon_-' = 2U - P. \qquad (A20)$$

Note, however, that the latter doublon band is unstable for nonzero k far enough from the Brillouin zone boundaries.

With the obtained rigorous solution, we can also find the condition for closing of the gap between two doublon bands. To this end, two roots for $\varepsilon(k = 0)$ given by Eqs. (A19) and (A20) should coincide, i.e.,

$$UP = -2J^2. \qquad (A21)$$

In a similar manner we examine the condition for a flat band. Inspecting Eqs. (A18), (A19), and (A20), we find out that $\varepsilon_+ = \varepsilon_-'$ and $\varepsilon_- = \varepsilon_+'$ provided

$$UP = -J^2. \qquad (A22)$$

Note that ε_+ and ε_+' can correspond to the same or to different doublon bands depending on the parameter choice, and the subscript $\pm$ is used here just to label the solutions.

Quite interestingly, both of these results, Eqs. (A21) and (A22), coincide with those obtained from the simplified SSH-type effective model, Eqs. (11) and (12). Additionally, we can find the conditions for collapse of the doublon state. The collapsing band is characterized by the decreased colocalization of photons, i.e., $x \to 0$. Solving Eqs. (A14) and (A15) for $k = 0$ with $x = 0$, we find the following condition:

$$2U - P = \pm 4J. \qquad (A23)$$

In a similar manner one can also examine the collapse of the doublon with arbitrary wave number k.

APPENDIX B: CALCULATION OF THE ZAK PHASE FOR BULK DOUBLON BANDS

The obtained analytic solution for the dispersion of doublons allows us to evaluate the Zak phase for bulk doublon bands. To this end, we take the periodic part $|u_k\rangle$ of the full doublon wave function in the form

$$|u_k\rangle = \beta_{0,0}|2_0\rangle + \beta_{1,1}|2_1\rangle + \sqrt{2}\sum_{n=1}^{\infty}\beta_{n,-n}|1_n 1_{-n}\rangle$$

$$+ \sqrt{2}\sum_{n=2}^{\infty}\beta_{n,2-n}|1_n 1_{2-n}\rangle + \frac{1}{\sqrt{2}}\sum_{n=1}^{\infty}\beta_{n-1,-n}|1_{n-1} 1_{-n}\rangle$$

$$+ \sqrt{2}\sum_{n=1}^{\infty}\beta_{n,1-n}|1_n 1_{1-n}\rangle + \frac{1}{\sqrt{2}}\sum_{n=1}^{\infty}\beta_{n+1,2-n}|1_{n+1} 1_{2-n}\rangle, \qquad (B1)$$

where $|1_m 1_n\rangle \equiv \hat{a}_m^\dagger \hat{a}_n^\dagger |0\rangle$ for $m \neq n$ and $|2_m\rangle \equiv 2^{-1/2}(\hat{a}_m^\dagger)^2 |0\rangle$. The corresponding choice of the unit cell is illustrated in Fig. 4(a). Importantly, this unit cell is inversion symmetric, which ensures quantization of the Zak phase in units of π [57].

In turn, the coefficients β_{mn} are defined from Eq. (A4) and hence

$$|u_k\rangle = C_1|v_1\rangle + C_2|v_2\rangle, \qquad (B2)$$

$$|v_1\rangle = |2_0\rangle + e^{ik}|2_1\rangle + \sqrt{2}\sum_{n=1}^{\infty}e^{i\varkappa_1 n}|1_n 1_{-n}\rangle$$

$$+ \sqrt{2}\sum_{n=2}^{\infty}e^{i\varkappa_1(n-1)}e^{ik}|1_n 1_{2-n}\rangle$$

$$+ \frac{1}{\sqrt{2}}\sum_{n=1}^{\infty}e^{i\varkappa_1(n-\frac{1}{2})}\Big[e^{-\frac{ik}{2}}|1_{n-1} 1_{-n}\rangle$$

$$+ 2e^{\frac{ik}{2}}|1_n 1_{1-n}\rangle + e^{\frac{3ik}{2}}|1_{n+1} 1_{2-n}\rangle\Big], \qquad (B3)$$

$$|v_2\rangle = |2_0\rangle - e^{ik}|2_1\rangle + \sqrt{2}\sum_{n=1}^{\infty}e^{i\varkappa_2 n}|1_n 1_{-n}\rangle$$

$$- \sqrt{2}\sum_{n=2}^{\infty}e^{i\varkappa_2(n-1)}e^{ik}|1_n 1_{2-n}\rangle$$

$$+ \frac{1}{\sqrt{2}}\sum_{n=1}^{\infty}e^{i\varkappa_2(n-\frac{1}{2})}\Big[-ie^{-\frac{ik}{2}}|1_{n-1} 1_{-n}\rangle$$

$$+ 2ie^{\frac{ik}{2}}|1_n 1_{1-n}\rangle - ie^{\frac{3ik}{2}}|1_{n+1} 1_{2-n}\rangle\Big]. \qquad (B4)$$

The Zak phase is defined in terms of the Berry connection as

$$\gamma = \int_{-\pi/2}^{\pi/2} A(k)\,dk, \qquad (B5)$$

where the Berry connection $A(k)$

$$A(k) = i\Big\langle u_k \Big| \frac{\partial u_k}{\partial k} \Big\rangle = iC_1^* \frac{\partial C_1}{\partial k}\langle v_1|v_1\rangle + iC_1^* \frac{\partial C_2}{\partial k}\langle v_1|v_2\rangle$$

$$+ iC_1^* C_1 \Big\langle v_1 \Big| \frac{\partial v_1}{\partial k} \Big\rangle + iC_1^* C_2 \Big\langle v_1 \Big| \frac{\partial v_2}{\partial k} \Big\rangle$$

$$+ iC_2^* \frac{\partial C_1}{\partial k}\langle v_2|v_1\rangle + iC_2^* \frac{\partial C_2}{\partial k}\langle v_2|v_2\rangle$$

$$+ iC_2^* C_1 \Big\langle v_2 \Big| \frac{\partial v_1}{\partial k} \Big\rangle + iC_2^* C_2 \Big\langle v_2 \Big| \frac{\partial v_2}{\partial k} \Big\rangle. \qquad (B6)$$

Using Eqs. (B3) and (B4), we calculate the scalar products

$$\langle v_1|v_1\rangle = \frac{2(1 + x_{11}) + 3\sqrt{x_{11}}}{1 - x_{11}}, \qquad (B7)$$

$$\langle v_1|v_2\rangle = \langle v_2|v_1\rangle^* = i\frac{\sqrt{x_{12}}}{1 - x_{12}}, \qquad (B8)$$

$$\langle v_2 | v_2 \rangle = \frac{2(1 + x_{22}) + 3\sqrt{x_{22}}}{1 - x_{22}}, \tag{B9}$$

$$\left\langle v_1 \middle| \frac{\partial v_1}{\partial k} \right\rangle = i \varkappa_1' \frac{8x_{11} + 3\sqrt{x_{11}}(1 + x_{11})}{2(1 - x_{11})^2}$$

$$+ i \frac{2(1 + x_{11}) + 3\sqrt{x_{11}}}{2(1 - x_{11})}, \tag{B10}$$

$$\left\langle v_1 \middle| \frac{\partial v_2}{\partial k} \right\rangle = -\frac{2i(1 + x_{12}) + \sqrt{x_{12}}}{2(1 - x_{12})}$$

$$- \varkappa_2' \frac{\sqrt{x_{12}}(1 + x_{12})}{2(1 - x_{12})^2}, \tag{B11}$$

$$\left\langle v_2 \middle| \frac{\partial v_1}{\partial k} \right\rangle = -\frac{2i(1 + x_{21}) - \sqrt{x_{12}}}{2(1 - x_{21})}$$

$$+ \varkappa_1' \frac{\sqrt{x_{21}}(1 + x_{21})}{2(1 - x_{21})^2}, \tag{B12}$$

$$\left\langle v_2 \middle| \frac{\partial v_2}{\partial k} \right\rangle = i \varkappa_2' \frac{8x_{22} + 3\sqrt{x_{22}}(1 + x_{22})}{2(1 - x_{22})^2}$$

$$+ i \frac{2(1 + x_{22}) + 3\sqrt{x_{22}}}{2(1 - x_{22})}, \tag{B13}$$

where $x_{\alpha\beta} = (e^{i\varkappa_\alpha})^* e^{i\varkappa_\beta}$.

The scalar products $\langle \frac{\partial v_i}{\partial k} | v_j \rangle$ are obtained by complex conjugation of $\langle v_j | \frac{\partial v_i}{\partial k} \rangle$. Calculating the Berry connection, we need to determine five quantities: $\frac{\partial C_1}{\partial k}$, $\frac{\partial C_2}{\partial k}$, $\frac{\partial \varkappa_1}{\partial k}$, $\frac{\partial \varkappa_2}{\partial k}$, and $\frac{\partial \varepsilon}{\partial k}$. Differentiation of the identities, Eqs. (A5)–(A8), with respect to k yields only four equations. One more equation can be obtained differentiating the identity

$$\langle u_k | u_k \rangle = 1, \tag{B14}$$

which is the normalization condition for the periodic part of the wave function. In these calculations, the gauge of the wave function should be fixed. To ensure smooth behavior of coefficients C_1 and C_2 with k, we choose their phases such that $(C_1 + C_2)e^{i\phi}$ is real, where

$$e^{i\phi} = \sqrt{\frac{-Pe^{-ik} - 2U + 4iJ \sin \varkappa_1/2 \cos k/2}{Pe^{ik} + 2U - 4iJ \sin \varkappa_1/2 \cos k/2}}. \tag{B15}$$

This choice ensures, in particular, that the Berry connection is a smooth function of the wave number k. The Zak phase calculation is then accomplished in several steps:

i. Complex coefficients $C_{1,2}$ are calculated using the normalization condition, Eq. (B14), and Eqs. (A9) and (A10).

ii. The derivatives $\frac{\partial C_1}{\partial k}$, $\frac{\partial C_2}{\partial k}$, $\frac{\partial \varkappa_1}{\partial k}$, $\frac{\partial \varkappa_2}{\partial k}$, and $\frac{\partial \varepsilon}{\partial k}$ are evaluated from the differentiated identities Eqs. (A5)–(A8) and (B14).

iii. The obtained quantities are inserted into Eq. (B6) and the Berry connection is evaluated numerically in the entire Brillouin zone. The Zak phase is recovered by numerical integration.

Performing the calculation of the Zak phase for different values of model parameters U and P, we plot the phase diagram shown in Fig. 4(b) and analyze topological transitions occurring in the system. For the unit cell choice shown in Fig. 4(a), the link with the direct two-photon hopping is located inside the unit cell. For $U > 1$, $\gamma = \pi$ is achieved exactly in the same range of parameters when $|j + P| < j$, i.e., the weak tunneling link appears *inside* the unit cell. This is consistent with the result expected from the effective SSH model with coupling constants equal to $j = J^2/U$ and $j + P$.

Quite importantly, the value of the Zak phase depends on the unit cell choice. Below, we briefly discuss what happens if the unit cell is chosen such that the P link is outside of the unit cell. To analyze this without repeating lengthy calculations, we note that the doublons in our problem are effectively 1D and hence their Hamiltonian can be effectively reduced to a 1D model sketched in Fig. 4(b). Assume that the periodic part of the wave function corresponding to the original unit cell choice reads $|\psi\rangle = (u_1, u_2)^T$. Then, if the unit cell is shifted by half a period, the wave function is modified as $|\psi'\rangle = (u_2, u_1 e^{ik})^T$, where $-\pi < k < \pi$, and the wave function is normalized to unity. As a result, the Berry connection calculated for the new wave function reads

$$A'(k) = A(k) - |u_1|^2. \tag{B16}$$

Furthermore, since the unit cell is inversion symmetric and the inversion operator has the form $\hat{P} = \sigma_x$, the periodic part
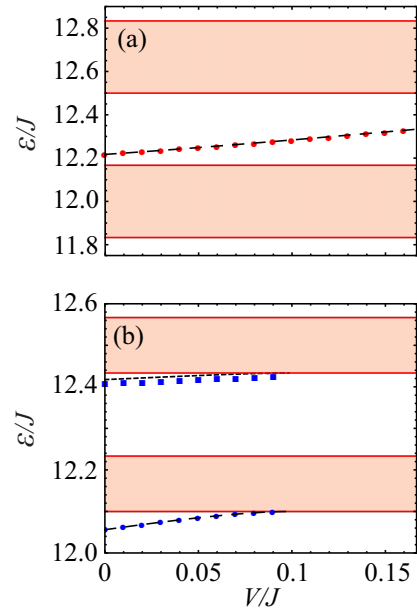

FIG. 5. Energies of doublon edge states versus additional potential V applied to the first site to compensate the interaction-induced detuning. Red-shaded areas highlight the range occupied by bulk doublon bands, dashed black lines show the prediction of the effective SSH model, and dots depict the results of exact diagonalization of the Hamiltonian for a finite array of 19 sites. (a) Topological case with $U/J = 6$ and $P/J = -0.5$ shown by point A in Fig. 4(c). (b) Trivial case with $U/J = 6$ and $P/J = -0.1$ shown by point C in Fig. 4(c).

of the wave function satisfies the condition

$$\begin{pmatrix} u_2(k) \\ u_1(k) \end{pmatrix} = e^{i\alpha(k)} \begin{pmatrix} u_1(-k) \\ u_2(-k) \end{pmatrix}, \qquad (B17)$$

i.e., $|u_2(k)| = |u_1(-k)|$. Hence, the Zak phase for the shifted unit cell choice

$$\gamma' = \gamma - \int_{-\pi}^{\pi} |u_1(k)|^2 \, dk$$

$$= \gamma - \int_0^{\pi} [|u_1(k)|^2 + |u_1(-k)|^2] \, dk$$

$$= \gamma - \int_0^{\pi} [|u_1(k)|^2 + |u_2(k)|^2] \, dk = \gamma - \pi, \quad (B18)$$

i.e., the Zak phase calculated for the shifted unit cell choice changes its value from π to 0 or from 0 to π modulo 2π.

Finally, it should be highlighted that, besides the analogy with the effective SSH model, our system also exhibits some distinctive properties. First, even if one of the doublon bands collapses, the Zak phase can still be defined using the wave functions for the remaining band. Furthermore, despite the collapse of the bulk doublon band, the doublon edge state can persist, which provides an interesting feature of two-photon edge states.

Even though this model is just a particular example, we believe that the present analysis provides valuable insights into the topological properties and bulk-boundary correspondence in nonlinear topological models.

APPENDIX C: DRAWING THE DISTINCTION BETWEEN TRIVIAL AND TOPOLOGICAL DOUBLON EDGE STATES

Since the considered model features both trivial and topological doublon edge states, it is important to draw a clear distinction between them. For this purpose, we calculate the spectrum of our model applying an additional detuning potential V to the first site of the array such that its two-photon energy is equal to $2U + j + V$ [cf. Eq. (8)]. Next we trace the evolution of doublon edge states when the magnitude of the detuning is gradually increased, reaching j and compensating the interaction-induced detuning of the edge site [cf. Eq. (6), (7)]. Two characteristic situations are observed.

In the first case, depicted in Fig. 5(a), the doublon edge state shifts towards the center of the doublon bandgap and appears exactly in the midgap position for $V = j$. This immediately clarifies the topological nature of this edge state, highlighting the analogy with its counterpart in the SSH model.

In the second scenario, shown in Fig. 5(b), two doublon edge states are present simultaneously, and one of them is again located inside the doublon bandgap. However, when the detuning V is increased, both of the edge states disappear, merging with the bulk doublon bands. Therefore, this pair of edge states should be identified with the trivial Tamm-like states.

Note that this analysis complements the Zak phase calculation highlighting the validity of the bulk-boundary correspondence principle for our two-particle model.

[1] L. Lu, J. D. Joannopoulos, and M. Soljačić, Topological photonics, Nat. Photon. **8**, 821 (2014).

[2] L. Lu, J. D. Joannopoulos, and M. Soljačić, Topological states in photonic systems, Nat. Phys. **12**, 626 (2016).

[3] A. B. Khanikaev and G. Shvets, Two-dimensional topological photonics, Nat. Photon. **11**, 763 (2017).

[4] T. Ozawa, H. M. Price, A. Amo, N. Goldman, M. Hafezi, L. Lu, M. C. Rechtsman, D. Schuster, J. Simon, O. Zilberberg, and I. Carusotto, Topological photonics, Rev. Mod. Phys. **91**, 015006 (2019).

[5] M. S. Rider, S. J. Palmer, S. R. Pocock, X. Xiao, P. A. Huidobro, and V. Giannini, A perspective on topological nanophotonics: Current status and future challenges, J. Appl. Phys. **125**, 120901 (2019).

[6] D. Smirnova, D. Leykam, Y. Chong, and Y. Kivshar, Nonlinear topological photonics, Appl. Phys. Rev. **7**, 021306 (2020).

[7] P. Roushan, C. Neill, Yu Chen, M. Kolodrubetz, C. Quintana, N. Leung, M. Fang, R. Barends, B. Campbell, Z. Chen, B. Chiaro, A. Dunsworth, E. Jeffrey, J. Kelly, A. Megrant, J. Mutus, P. J. J. O'Malley, D. Sank, A. Vainsencher, J. Wenner, T. White, A. Polkovnikov, A. N. Cleland, and J. M. Martinis, Observation of topological transitions in interacting quantum circuits, Nature **515**, 241 (2014).

[8] S. Barik, A. Karasahin, C. Flower, T. Cai, H. Miyake, W. DeGottardi, M. Hafezi, and E. Wacks, A topological quantum optics interface, Science **359**, 666 (2018).

[9] J.-L. Tambasco, G. Corrielli, R. J. Chapman, A. Crespi, O. Zilberberg, R. Osellame, and A. Peruzzo, Quantum interference of topological states of light, Sci. Adv. **4**, eaat3187 (2018).

[10] S. Mittal, E. A. Goldschmidt, and M. Hafezi, A topological source of quantum light, Nature **561**, 502 (2018).

[11] A. Blanco-Redondo, B. Bell, D. Oren, B. J. Eggleton, and M. Segev, Topological protection of biphoton states, Science **362**, 568 (2018).

[12] Y. Wang, X.-L. Pang, Y.-H. Lu, J. Gao, Y.-J. Chang, L.-F. Qiao, Z.-Q. Jiao, H. Tang, and X.-M. Jin, Topological protection of two-photon quantum correlation on a photonic chip, Optica **6**, 955 (2019).

[13] K. Wang, J. G. Titchener, S. S. Kruk, L. Xu, H.-P. Chung, M. Parry, I. I. Kravchenko, Y.-H. Chen, A. S. Solntsev, Y. S. Kivshar, D. N. Neshev, and A. A. Sukhorukov, Quantum metasurface for multiphoton interference and state reconstruction, Science **361**, 1104 (2018).

[14] M. C. Rechtsman, Y. Lumer, Y. Plotnik, A. Perez-Leija, A. Szameit, and M. Segev, Topological protection of photonic path entanglement, Optica **3**, 925 (2016).

[15] S. Mittal, V. V. Orre, and M. Hafezi, Topologically robust transport of entangled photons in a 2D photonic system, Opt. Express **24**, 15631 (2016).

[16] D. C. Mattis, The few-body problem on a lattice, Rev. Mod. Phys. **58**, 361 (1986).

[17] K. Winkler, G. Thalhammer, F. Lang, R. Grimm, J. Hecker Denschlag, A. J. Daley, A. Kantian, H. P. Buchler, and P. Zoller, Repulsively bound atom pairs in an optical lattice, Nature **441**, 853 (2006).

[18] M. Valiente and D. Petrosyan, Two-particle states in the Hubbard model, J. Phys. B **41**, 161002 (2008).

[19] M Valiente and D Petrosyan, Scattering resonances and two-particle bound states of the extended Hubbard model, J. Phys. B **42**, 121001 (2009).

[20] C. Menotti, F. Minganti, and A. Recati, Momentum-dependent pseudospin dimers of coherently coupled bosons in optical lattices, Phys. Rev. A **93**, 033602 (2016).

[21] M. Bello, C. E. Creffield, and G. Platero, Sublattice dynamics and quantum state transfer of doublons in two-dimensional lattices, Phys. Rev. B **95**, 094303 (2017).

[22] Y.-M. Wang and J.-Q. Liang, Repulsive bound-atom pairs in an optical lattice with two-body interaction of nearest neighbors, Phys. Rev. A **81**, 045601 (2010).

[23] R. A. Pinto, J. P. Nguenang, and S. Flach, Boundary effects on quantum q-breathers in a Bose-Hubbard chain, Physica D **238**, 581 (2009).

[24] R. A. Pinto, M. Haque, and S. Flach, Edge-localized states in quantum one-dimensional lattices, Phys. Rev. A **79**, 052118 (2009).

[25] J. M. Zhang, D. Braak, and M. Kollar, Bound States in the Continuum Realized in the One-Dimensional Two-Particle Hubbard Model with an Impurity, Phys. Rev. Lett. **109**, 116405 (2012).

[26] J. M. Zhang, D. Braak, and M. Kollar, Bound states in the one-dimensional two-particle Hubbard model with an impurity, Phys. Rev. A **87**, 023613 (2013).

[27] S. Longhi and G. Della Valle, Tamm-Hubbard surface states in the continuum, J. Phys. Condens. Matter **25**, 235601 (2013).

[28] M. A. Gorlach and A. N. Poddubny, Interaction-induced two-photon edge states in an extended Hubbard model realized in a cavity array, Phys. Rev. A **95**, 033831 (2017).

[29] M. Di Liberto, A. Recati, I. Carusotto, and C. Menotti, Two-body bound and edge states in the extended SSH Bose-Hubbard model, Eur. Phys. J. Special Topics **226**, 2751 (2017).

[30] G. Salerno, M. Di Liberto, C. Menotti, and I. Carusotto, Topological two-body bound states in the interacting Haldane model, Phys. Rev. A **97**, 013637 (2018).

[31] G. Salerno, G. Palumbo, N. Goldman, and M. Di Liberto, Interaction-induced lattices for bound states: Designing flat bands, quantized pumps, and higher-order topological insulators for doublons, Phys. Rev. Res. **2**, 013348 (2020).

[32] J. Tangpanitanon, V. M. Bastidas, S. Al-Assam, P. Roushan, D. Jaksch, and D. G. Angelakis, Topological Pumping of Photons in Nonlinear Resonator Arrays, Phys. Rev. Lett. **117**, 213603 (2016).

[33] Y. Ke, X. Qin, Y. S. Kivshar, and C. Lee, Multiparticle Wannier states and Thouless pumping of interacting bosons, Phys. Rev. A **95**, 063630 (2017).

[34] M. Lyubarov and A. Poddubny, Exceptional points for photon pairs bound by nonlinear dissipation in cavity arrays, Opt. Lett. **43**, 5917 (2018).

[35] W. P. Su, J. R. Schrieffer, and A. J. Heeger, Solitons in Polyacetylene, Phys. Rev. Lett. **42**, 1698 (1979).

[36] M. Di Liberto, A. Recati, I. Carusotto, and C. Menotti, Two-body physics in the Su-Schrieffer-Heeger model, Phys. Rev. A **94**, 062704 (2016).

[37] M. A. Gorlach and A. N. Poddubny, Topological edge states of bound photon pairs, Phys. Rev. A **95**, 053866 (2017).

[38] A. M. Marques and R. G. Dias, Topological bound states in interacting Su-Schrieffer-Heeger rings, J. Phys. Condens. Matter **30**, 305601 (2018).

[39] Y. Hadad, A. B. Khanikaev, and A. Alù, Self-induced topological transitions and edge states supported by nonlinear staggered potentials, Phys. Rev. B **93**, 155112 (2016).

[40] Y. Hadad, V. Vitelli, and A. Alù, Solitons and propagating domain walls in optical resonator arrays, ACS Photon. **4**, 1974 (2017).

[41] Y. Hadad, J. C. Soric, A. B. Khanikaev, and A. Alù, Self-induced topological protection in nonlinear circuit arrays, Nat. Electron. **1**, 178 (2018).

[42] N. A. Olekhno, E. I. Kretov, A. A. Stepanenko, P. A. Ivanova, V. V. Yaroshenko, E. M. Puhtina, D. S. Filonov, B. Cappello, L. Matekovits, and M. A. Gorlach, Topological edge states of interacting photon pairs emulated in a topolectrical circuit, Nat. Commun. **11**, 1436 (2020).

[43] Y. Lumer, Y. Plotnik, M. C. Rechtsman, and M. Segev, Self-Localized States in Photonic Topological Iinsulators, Phys. Rev. Lett. **111**, 243905 (2013).

[44] D. Leykam and Y. D. Chong, Edge Solitons in Nonlinear-Photonic Topological Insulators, Phys. Rev. Lett. **117**, 143901 (2016).

[45] O. Bleu, G. Malpuech, and D. D. Solnyshkov, Robust quantum valley Hall effect for vortices in an interacting bosonic quantum fluid, Nat. Commun. **9**, 3991 (2018).

[46] O. Dutta, M. Gajda, P. Hauke, M. Lewenstein, D.-S. Lühmann, B. A. Malomed, T. Sowiński, and J. Zakrzewski, Non-standard Hubbard models in optical lattices: A review, Rep. Prog. Phys. **78**, 066001 (2015).

[47] P. Roushan, C. Neill, A. Megrant, Y. Chen, R. Babbush, R. Barends, B. Campbell, Z. Chen, B. Chiaro, A. Dunsworth *et al.*, Chiral ground-state currents of interacting photons in a synthetic magnetic field, Nat. Phys. **13**, 146 (2017).

[48] P. Roushan, C. Neill, J. Tangpanitanon, V. M. Bastidas, A. Megrant, R. Barends, Y. Chen, Z. Chen, B. Chiaro, A. Dunsworth *et al.*, Spectroscopic signatures of localization with interacting photons in superconducting qubits, Science **358**, 1175 (2017).

[49] Y. Ye, Z.-Y. Ge, Y. Wu, S. Wang, M. Gong, Y.-R. Zhang, Q. Zhu, R. Yang, S. Li, F. Liang, J. Lin, Y. Xu, C. Guo, L. Sun, C. Cheng, N. Ma, Z. Y. Meng, H. Deng, H. Rong, C.-Y. Lu, C.-Z. Peng, H. Fan, X. Zhu, and J.-W. Pan, Propagation and Localization of Collective Excitations on a 24-Qubit Superconducting Processor, Phys. Rev. Lett. **123**, 050502 (2019).

[50] M. Kounalakis, C. Dickel, A. Bruno, N. K. Langford, and G. A. Steele, Tuneable hopping and nonlinear cross-Kerr interactions in a high-coherence superconducting circuit, npj Quantum Info. **4**, 38 (2018).

[51] J. Zurita, C. E. Creffield, and G. Platero, Topology and interactions in the photonic Creutz and Creutz-Hubbard aldders, Adv. Quantum Technol. **3**, 1900105 (2020).

[52] S. Mukherjee, M. Valiente, N. Goldman, A. Spracklen, E. Andersson, P. Öhberg, and R. R. Thomson, Observation of pair tunneling and coherent destruction of tunneling in arrays of optical waveguides, Phys. Rev. A **94**, 053853 (2016).

[53] A. Blanco-Redondo, I. Andonegui, M. J. Collins, G. Harari, Y. Lumer, M. C. Rechtsman, B. J. Eggleton, and M. Segev, Topological Optical Waveguiding in Silicon and the Transition Between Topological and Trivial Defect States, Phys. Rev. Lett. **116**, 163901 (2016).

[54] F. H. L. Essler, H. Frahm, F. Gohmann, A. Klumper, and V. E. Korepin, *The One-Dimensional Hubbard Model* (Cambridge University Press, Cambridge, UK, 2005).

[55] M. Karbach and G. Muller, Introduction to the Bethe ansatz I, Computers Phys. **11**, 36 (1997).

[56] C. W. Hsu, B. Zhen, A. D. Stone, J. D. Joannopoulos, and M. Soljačić, Bound states in the continuum, Nat. Rev. Mater. **1**, 16048 (2016).

[57] J. Zak, Berry's Phase for Energy Bands in Solids, Phys. Rev. Lett. **62**, 2747 (1989).